Lithium-Ion Battery State-of-Charge Balancing with State-of-Health Awareness Capability

G.Esha Voruganti Bharath Kumar

Assistant Professor in EEE Department, St. Martin's Engineering College (Autonomous), Secunderabad-500100, INDIA

Assistant Professor in EEE Department, St. Martin's Engineering College (Autonomous), Secunderabad-500100, INDIA

***Abstract*—A state-of-charge (SOC) balancing method which accounts for state-of-health (SOH) status of battery cells is presented in this article. The data collected from aging experiments conducted in the laboratory indicates that there is correlation between the minimum impedance of the battery and capacity fading which can be used to predict capacity capability of the battery. However, this relationship is complex and nonlinear. In this article, artificial neural network (ANN) is utilized to learn this relationship and an ANN-based capacity estimator is developed to predict available capacity of battery cells. An online impedance measurement method with improved measurement resolution is presented to obtain a more accurate minimum impedance for the ANN-based capacity estimator. The estimated capacity from the ANN capacity estimator is fed to an SOC balancing controller to calculate SOC values for the battery cells. A battery cell with worse health has lower available capacity than a battery cell with better health, and, therefore, its SOC value is adjusted to a smaller value when SOH or capacity estimation functionality is activated. Because of this mechanism and the control principle of the presented SOC balancing controller, the system draws energy at a slower rate from the battery cell(s) with lower SOH and draws energy at a faster rate from the battery cell(s) with higher SOH such that all battery cells reach their end of discharge at the same time. This results in extending operation time of the system, makes best use of energy from every battery cell, and avoids over-discharging battery cells with lower SOH. The presented method is evaluated using results obtained from a laboratory experimental setup.**

***Index Terms*—Battery, battery balancing, battery capacity, battery management system (BMS), dc–dc, electrochemical impedance spectrum, power converter, state-of-charge (SOC), state-of-health (SOH).**

I. Introduction

BATTERIES and battery systems are widely used for energy storage in a wide range of applications such as consumer electronics, medical-portable electronic devices, automotive/vehicles, and smart grid [1]–[6]. Therefore, developing high-performance advanced battery management systems (BMSs) with crucial functions such as state-of-health (SOH) estimation and state-of-charge (SOC) estimation and balancing is important [7]–[27]. These functions allow to have an efficient, safe, and reliable battery system in the related application.

There are a variety of batteries' SOC balancing methods presented in the literature to address the SOC imbalance issue such as those presented in [10]–[21]. These methods can be classified into two main categories: 1) passive balancing scheme and 2) active balancing schemes [10]–[21]. Passive balancing scheme uses shunt resistors or switches which are connected in parallel with batteries to dissipate power [10], [11]. This scheme is simple to implement, but it wastes energy in order to achieve SOC balancing. On the other hand, active balancing schemes balance SOC through energy-recovery mechanisms [12]–[21] or energy drawing allocation control method (for instance, the energy sharing controller presented in [12]). Active SOC balancing schemes increase the energy utilization efficiency but are usually more complex to realize.

The aforementioned battery balancing schemes do not take the effect of the SOH of battery cells into account when performing SOC balancing. These SOC balancing schemes operate under the assumption that all of the battery cells or modules have the same capacity capability (same SOH), which cannot be guaranteed and might not be always the case. When a battery cell goes through more aging cycles, capacity fading and impedance growth will occur [22]–[27]. Battery cells or modules in a battery system might age differently, which results in different capacity fading rates or levels. If an SOC balancing controller assumes that all battery cells or modules have the same capacity as they age, then the battery cell or module with higher capacity fading (lower capacity value) may run out of charges (reach end of discharge condition) earlier than other battery cells or modules in the system. Under such situation, if the BMS continues to draw energy or charges from the aged battery cell or module, this battery cell or module will be subjected to over-discharging which might cause failure in the system and/or fire.

SOH estimation or capacity estimation methods can be classified into two main categories: 1) equivalent model-based methods and 2) data-driven methods [22]–[27]. The equivalent model-based methods include the electrochemical equivalent model method and electrical equivalent circuit model method [22]–[26]. Electrochemical equivalent model methods use complex differential equations to characterize the electrochemical reaction processes that occur inside the battery, which usually requires high computation power (and cost) in order to obtain the needed analytical solutions. The electrical equivalent circuit

Ms G.Esha has been working as an Assistant Professor in the Department ofElectrical and Electronics Engineering, St. Martin's Engineering College, Dhulapally Kompally, Secunderabad, Telangana, since last 2 Yearr. She was completed his M.Tech in the specialization of Powrer Electronics from Gokaraju rangaraju engineering college, affiliated to JNTUH Hyderabad, Telangana in 2015.

model methods usually use electric circuit component interconnections and values that can fit the electrochemical impedance spectroscopy (EIS) data. The equivalent model-based methods help to understand the underlying aging mechanism of a battery, which usually cannot be accurately generalized for other battery-type cells. When it comes to a new type of battery, the model has to be redeveloped almost completely to characterize the behavior of this new battery. Recently, data-driven methods become increasingly popular due to new developments of deep learning methods and developments of microprocessors/microcomputers with high computational capabilities and reduced size, cost, and power consumption [27]. Deep learning methods can learn the aging patterns based on historical data and then make prediction about the health status of a battery by taking input data from the process (new) measurement results of the battery.

This article presents a method which takes into account the effect of different SOH conditions for different battery cells or modules when balancing SOC. Aging data is collected in the laboratory for Li-Ion batteries and then analyzed. The collected and analyzed data includes EIS and capacity fading for the batteries. The collected data verified an existing correlation or relationship between the minimum magnitude value of the complex impedance ($Z_{\min}$) of the battery and capacity fading.

Since capacity fading indicates SOH status of the battery, it is found that $Z_{\min}$ has a very good potential to reflect the health status of battery. However, this relationship is nonlinear. Because of the strong nonlinear fitting capability and adaptability of artificial neural network (ANN), it is utilized to learn this nonlinear relationship between the SOH of the battery and $Z_{\min}$ and then to predict the SOH or the capacity capability of each battery cell or module. The capacity capability here refers to the amount of charges the battery can supply to the load when the battery is charged fully before it reaches the end of discharge condition. The presented ANN can adapt to the new changes in the battery cells behavior when new aging data is fed back into the ANN, which results in more accurate results compared with static aging prediction model.

The input data of the ANN, i.e., the minimum magnitude value of the complex impedance ($Z_{\min}$), is obtained or tracked by using the presented online impedance measurement method in this article with improved speed and accuracy compared with the methods in [28] and [29]. The capacity capability information of each battery cell from ANN estimator is fed into the SOC balancing module to calculate or adjust the SOC values. Based on the updated or corrected capacity capability, the system adjusts the SOC value of unhealthy battery to a smaller value compared with other relatively healthier batteries. This operation enables the system to draw higher energy from the healthier battery cells and/or smaller energy from the relatively less healthy battery cells, which allows to discharge battery cells/modules almost completely at the same time and extend the system operation time (and therefore efficiency) without over-discharging any of the battery cells or modules. Otherwise, it would likely result in further degrading the relatively less healthy battery cells, destroying them, or, in the worst case, causing them to catch fire.

The remainder of this article is organized as follows. Section II discusses the details of the principle of the presented SOH-aware SOC balancing method. The preliminary experimental evaluation results are presented in Section III. The conclusion is given in Section IV.

II. Principle of the SOH-Aware SOC Balancing Method

Fig. 1 shows an illustration diagram for the developed BMS used to evaluate the presented SOC balancing controller with SOH awareness capability. The distributed battery architecture is adopted, i.e., each battery cell (or each module consisting of several battery cells) is connected to its own low-voltage dc–dc converter instead of using one single high-voltage high-power dc–dc converter for all in series connected cells [12]. Each battery cell and its dc–dc converter are connected together to form a battery power unit (BPU). The BPUs are connected in series at the output of the power converters to form a battery pack. There are three main modules in this BMS (each module represents one of the contributions of this article): 1) the ANN-based SOH estimation module, 2) the module used for tracking of the minimum magnitude value of the complex impedance for each battery cell or module, and (3) the SOC balancing module. These three modules are discussed in the remainder of this section.

A. ANN-Based SOH Estimation Module

The adopted definition for SOH in this article is based on capacity fading, as given by the following equation:

$$\mathrm{SOH} = \frac{Q_{\mathrm{avail}}}{Q_{\mathrm{nominal}}} \tag{1}$$

where Q_{avail} is the amount of available charges the fully charged battery cell can supply under the current health condition, and Q_{nominal} is the nominal amount of charges the fully charged battery cell can supply when it is new. Q_{avail} can be experimentally measured during battery discharging operation, and Q_{nominal} can usually be obtained from the manufacturer's datasheet (or can also be measured experimentally when the battery is new). When the battery is new, $Q_{\mathrm{avail}} = Q_{\mathrm{nominal}}$ and therefore $\mathrm{SOH} = 1$ or 100%.

In order to calculate the SOH value as defined in (1), there is a need to obtain the value of Q_{avail}. In this article, an ANN-based capacity estimator is developed to estimate the value of Q_{avail}.

Fig. 2 illustrates the correlation between the value of minimum magnitude of complex impedance of lithium-ion battery cell (Tenergy ICR lithium-ion battery 18650-2600) and the value of Q_{avail} at different SOC conditions (i.e., at 100%, 60%, and 20% SOC here) as the battery cell ages. The battery minimum impedance may be different at different SOC conditions as the results obtained by the authors showed and as discussed in the literature [28]–[30]. The minimum magnitude of battery impedance is measured at fully charged state (100% SOC state) in this article to reduce the effect of SOC on the measurement of $Z_{\min}$. Fig. 2 is based on aging data that is collected by charge/discharge cycling of lithium-ion battery cells [5]. The lithium-ion battery cells are aged by using 1 C (i.e., 2.6 A) constant discharging rate and 1 C constant current charging rate

Mr.S Kalangi Balasubramanyam has been working as an Assistant Professor in the Department of Electronics and Communication Engineering, St. Martin's Engineering College, Dhulanally, Kompally, Secunderabad, Telangana, since last 6 months. He was completed his M.Tech in the specialization of Embedded systems from Laqshya Institute of Technology and Sciences, Khammam affiliated to JNTUH Hyderabad, Telangana in 2015 and he was completed his B.Tech in Electronics and Communication Engineering in 2012 from Swarna Bharathi College of Engineering, Khammam Affiliated to JNTUH, Hyderabad Telangana. He has published 7 research papers in reputed international journals. His total experience in teaching is 5 years.

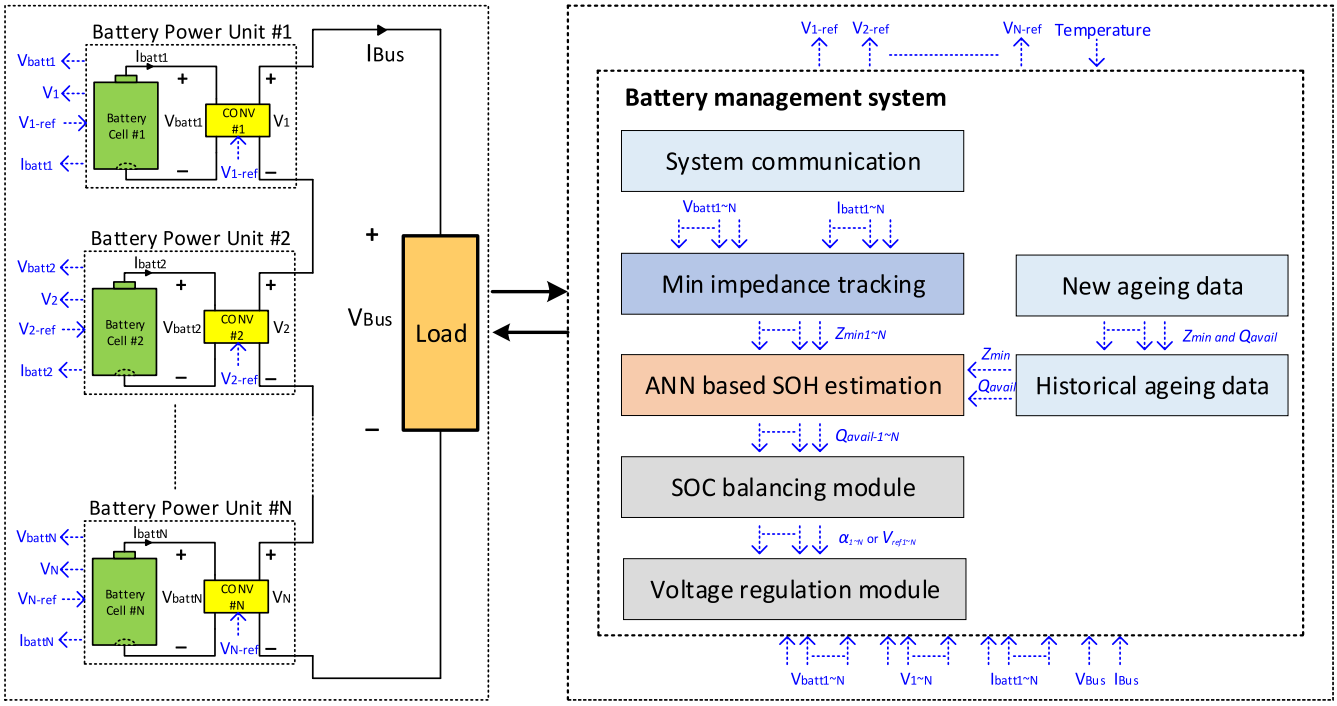

Fig. 1. Block diagram of the developed battery management system utilized to evaluate the presented SOC balancing method with SOH awareness capability.

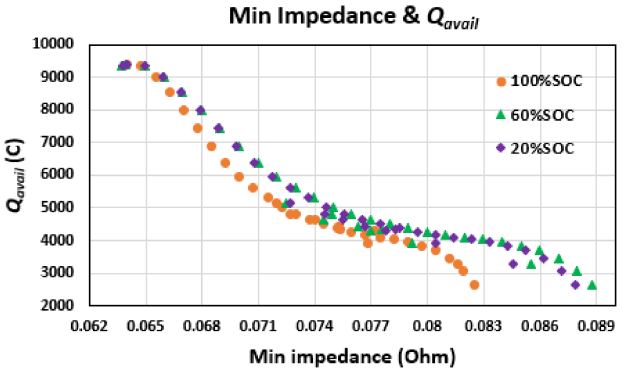

Fig. 2. Experimentally measured data that illustrates the correlation/relationship between minimum complex impedance magnitude value ($Z_{\min}$) and the value of Q_{avail} as the battery cell ages at different SOC conditions.

followed by a constant voltage charging operation mode. During each aging cycle, EIS data, battery voltage, battery current, and the charging/discharging time duration are measured and recorded.

From Fig. 2, it can be observed that the minimum impedance value of the lithium-ion battery (i.e., $Z_{\min}$) has a clear and strong correlation with SOH which indicates how many charges (i.e., Q_{avail}) the battery can supply to its load especially at 100% SOC condition (when the battery is fully charged). This correlation is strongly supported by the accelerated aging experiments that were carried out as a part of this work. The relationship between $Z_{\min}$ and Q_{avail} is not a simple linear one. Therefore, the ANN, as a powerful fitting tool for nonlinear complex data, is utilized in this article to model or learn the complex and nonlinear relationship between $Z_{\min}$ and the SOH of the battery. It should be noted that the ANN-based capacity estimator utilizes the minimum impedance value regardless of the frequency value at which it occurs at.

Fig. 3 shows the flowchart of the presented ANN-based battery capacity estimator using battery cell EIS. The historical data together with new data from the latest cycle measurements are bonded as the battery aging dataset. Data cleansing is performed which mainly removes the outliers in the dataset. Then the data is standardized such that it can be fed into the neural network. The standardization is done by using the following equation [33]:

$$x' = \frac{x - \mu}{\sigma} \tag{2}$$

where x' is the data after standardization, x is the original input data, μ is the mean value of the input data, and σ is the standard deviation of the input data. After the standardization step, the dataset is split into *k*-fold cross-validation set and test set [34]. The *k*-fold cross-validation technique is used here to guide the training of ANN model. If the average validation error is below a specified threshold value, then the training of neural network is considered to be complete and the trained ANN model is evaluated using the test data. Otherwise, the hyperparameters of the ANN model have to be tuned to obtain better cross-validation score. This is an iterative process to find the optimum parameter values for the ANN model.

The structure used by the presented ANN-based capacity estimator in this article includes: one input layer, two hidden layers, and one output layer. These layers are stacked sequentially with fully connected structure. The input is the minimum value of the

TABLE I
COMPARISON BETWEEN ANN, LOOKUP TABLE METHOD AND CURVE FITTING METHOD

Methods	Advantages	Disadvantages
Look-up table [31]	Easy to create; low hardware requirements and computation cost.	Discrete points/values and poor interpolation and extrapolation performance. For example, when the data point (Z_{min1}, Q_{avail1}) is not stored in the look-up table, the corresponding value of Q_{avail1} for Z_{min1} is approximated as to be the next closest point Q_{avail2} in the look-up table which corresponds to Z_{min2}. Require large memory resources because of storing large number of data points.
Curve fitting [32]	Continuous mapping/modeling; relatively easy to create; low hardware requirements and computation cost.	Poor accuracy when used for nonlinear fitting, poor expressive capability to model complex relationships, and poor upgradability when compared with ANN.
ANN [32]	Continuous mapping/modeling; strong and accurate nonlinear fitting and expressive capability to model or capture complex relationships; excellent scalability and upgradability [32].	Might require relatively higher hardware requirements and computation cost.

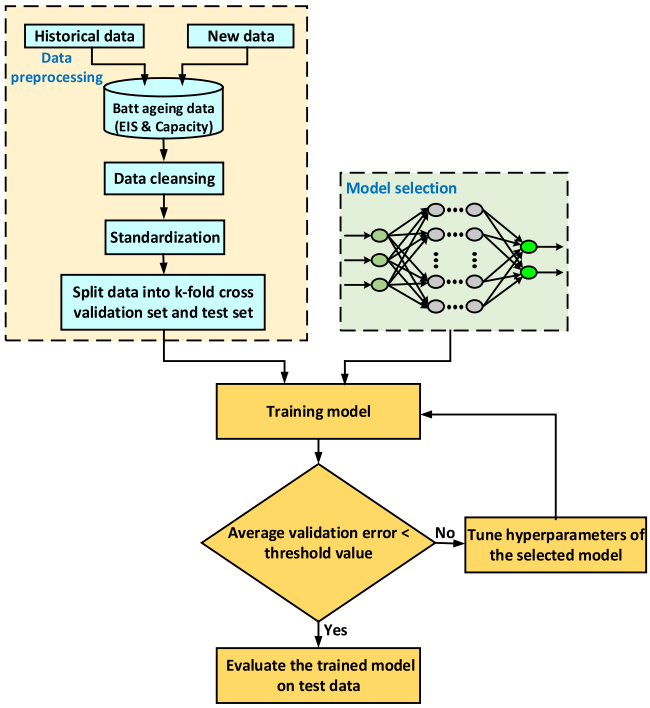

Fig. 3. Flowchart of ANN-based battery capacity estimator using EIS data.

complex impedance magnitude, i.e., $Z_{\min}$, for a fully charged battery cell. There are 64 neurons used in each hidden layer, and the activation function of the hidden layer is "RELU" function [35]. The output layer has no activation function, and it will output the estimated available capacity Q_{avail}. The loss function used for training the ANN is "*MSE*" as given by the following equation [36]:

$$MSE = \frac{1}{n}\sum_{i=1}^{n}(y_i - \tilde{y}_i)^2 \tag{3}$$

where n is the number of data points used to train the ANN, y_i is the value of Q_{avail} obtained from battery aging experiment, and $\tilde{y}_i$ is the predicted Q_{avail} value for the ith sample. The used optimizer of ANN model is "optimizer of ANN model is root mean square propagation (RMSPROP) algorithm" [37]. The RMSPROP algorithm is the optimization strategy to find the optimum parameter values of the model (e.g., weight and bias) to have the minimum value of the defined loss function, which is *MSE* function in this article.

Other data fitting methods, such as lookup table method [31] and curve fitting method [32], can also be used to model the correlation or relationship shown in Fig. 2. However, the ANN-based method has advantages over the lookup table method and the curve fitting method, as summarized in Table I, which yields better performance in terms of accuracy and upgradability/adaptability to evolving complex and dynamic battery operation conditions (e.g., at different SOC and temperature values) if needed in future work/update [32]. As the number of independent variables (or input variables) is increased, it is easier and more accurate for ANN to model relationships that involve many variables compared to the lookup table and curve fitting method. Moreover, the curve fitting method has poor accuracy when used to model highly nonlinear relationships and the accuracy of the lookup table method suffers due to the use of discrete data point values.

B. High-Speed Minimum Impedance Magnitude Tracking

Tracking the value of minimum complex impedance magnitude, i.e., $Z_{\min}$, of the battery is a critical part of the presented ANN-based capacity estimator since it is the input variable of the capacity estimator discussed in Section II-A. Fig. 4(a) illustrates the basic circuit diagram of the online EIS measurement methods [28], [29] used for tracking the value of $Z_{\min}$. The principle of the used impedance measurement method is based on the perturbation concept presented in [28] and [29]. The output voltage of the dc–dc converter that is connected to each battery cell is perturbed at the frequency of interest (at which the impedance measurement is to be measured). A sample impedance magnitude measurement result (with wide frequency range) for the battery cell used in this article is shown in Fig. 4(b) [28].

From Fig. 4(b), it can be observed that the magnitude of the impedance has a parabolic shape with an identifiable minimum value. The magnitude of impedance first decreases starting from low frequency to a certain minimum value at a given frequency, and then increases as the frequency value increases. Based on this characteristic of the battery impedance magnitude, the

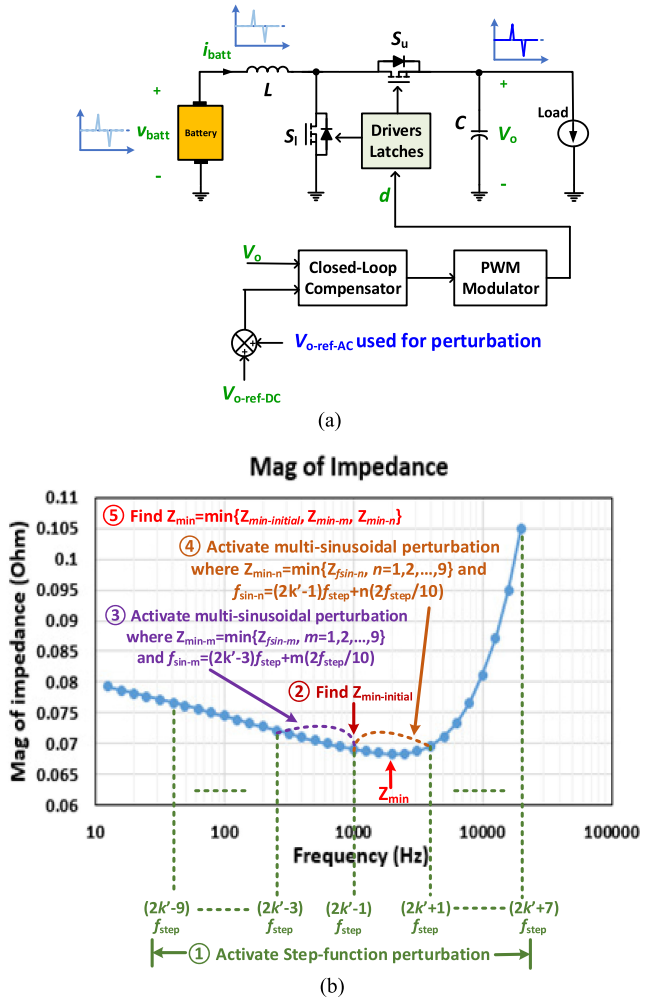

Fig. 4. Online EIS measurement for tracking minimum impedance ($Z_{\min}$) of battery [28], [29]. (a) Basic circuit diagram utilized for online EIS measurement. (b) Sample impedance magnitude measurement result for the battery cell used in this article [28].

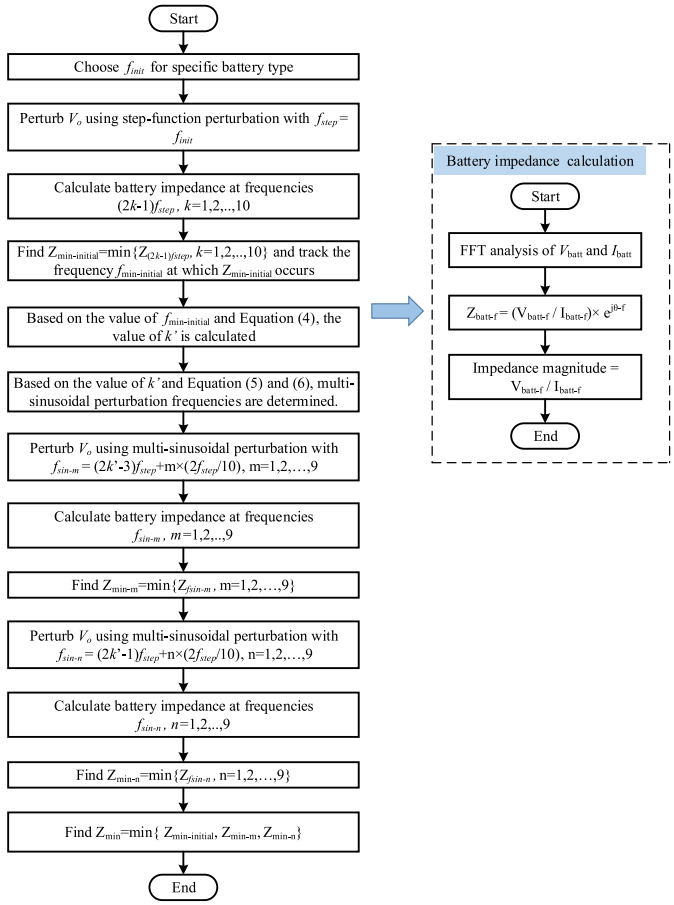

Fig. 5. Flowchart of the presented algorithm used to track the minimum complex impedance magnitude of the battery.

flowchart of the algorithm used to track the value of the minimum complex impedance magnitude is shown in Fig. 5. Fig. 4(b) shows a diagram that illustrates the process of tracking the minimum complex impedance magnitude of each battery. This process can be divided into the following steps.

Step 1: The step-function perturbation at frequency f_{step} is activated in the dc–dc converter. The selection of f_{step} is based on the type of battery and *a priori* knowledge about the battery. The battery impedance at the odd harmonics of f_{step}, i.e., $(2k - 1)\, f_{\text{step}}$, can be measured or obtained by using the battery impedance calculation procedure shown in Fig. 5. Because of the attenuation at higher order harmonics as discussed in [28], only the first 10 harmonics are utilized to calculate battery impedance in order to have accurate measurement results, i.e., k has a range from 1 to 10.

Step 2: A rough initial estimate for the minimum impedance value $Z_{\text{min-initial}}$ of the battery is found by comparing the acquired impedance values for the 10 harmonics from Step 1. The frequency at which $Z_{\text{min-initial}}$ occurs is denoted as $f_{\text{min-initial}} = (2k' - 1)f_{\text{step}}$, and then the value of k' can be determined based on (4). The value of k' is used to calculate the sinusoidal perturbation frequencies as given by (5) and (6). Because of the parabolic distribution characteristics of the impedance magnitude as shown in Fig. 4(b), the more accurate (or with better resolution) minimum impedance value should occur between the frequency ranges from $(2k' - 3)f_{\text{step}}$ to $(2k' - 1)f_{\text{step}}$ and from $(2k' - 1)f_{\text{step}}$ to $(2k'+ 1)\, f_{\text{step}}$, which is the reason why multisinusoidal perturbations are activated (following the step-function perturbation) within these two frequency ranges to track a more accurate minimum impedance value.

$$k' = \frac{f_{\text{min-initial}}}{2f_{\text{step}}} + \frac{1}{2} \tag{4}$$

$$f_{\text{sin}-m} = (2k' - 3)\, f_{\text{step}} + m \times \left(\frac{2f_{\text{step}}}{10}\right), \quad m = 1, 2, \ldots, 9. \tag{5}$$

$$f_{\text{sin}-n} = (2k' - 1)\, f_{\text{step}} + n \times \left(\frac{2f_{\text{step}}}{10}\right), n = 1, 2, \ldots, 9. \tag{6}$$

Step 3: The multisinusoidal perturbation within the frequency range from $(2k' - 3)f_{\text{step}}$ to $(2k' - 1)f_{\text{step}}$ is activated in the

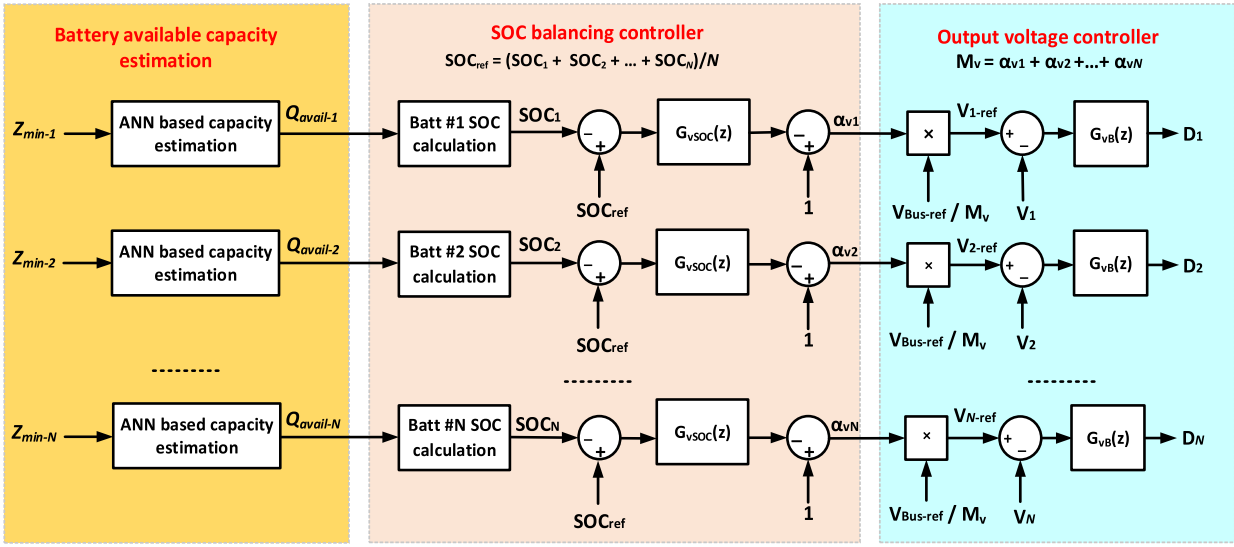

Fig. 6. Control diagram of the presented SOC balancing method considering the effect of SOH of battery cells.

dc–dc converter. The perturbation frequencies are calculated based on (5). Then the local minimum impedance value ($Z_{\text{min-}m}$) within the frequency range from $(2k'-3)f_{\text{step}}$ to $(2k'-1)f_{\text{step}}$ is obtained by comparing the impedance values at these sinusoidal perturbation frequencies. The value of m is chosen to be 9 in the experimental prototype of paper, but if higher resolution or more accurate minimum impedance measurement result is desired, m can be set to a larger value.

Step 4: The multisinusoidal perturbation within the frequency range from $(2k'-1)f_{\text{step}}$ to $(2k'+1)f_{\text{step}}$ is activated in the dc−dc converter. The perturbation frequencies are calculated based on (6). The local minimum impedance value (i.e., $Z_{\text{min-}n}$) within this frequency range is obtained by using the same procedure for tracking $Z_{\text{min-}m}$ as in Step 3.

Step 5: The final tracked minimum impedance magnitude value of the battery, i.e., Z_{min}, is obtained by comparing the values of $Z_{\text{min-initial}}$, $Z_{\text{min-}m}$, and $Z_{\text{min-}n}$. The Z_{min} value is equal to the smallest value among $Z_{\text{min-initial}}$, $Z_{\text{min-}m}$, and $Z_{\text{min-}n}$.

This hybrid approach of measuring the impedance which combines step-function perturbation [28] and sinusoidal perturbation [29] yields a more accurate minimum impedance value in shorter time before the battery condition changes. The step-function perturbation is used to quickly obtain the information about which frequency range Z_{min} is located within and the multisinusoidal perturbation is used to zoom in to find a more accurate value for Z_{min}.

C. SOC Balancing Module

Fig. 6 shows the control diagram of the SOC balancing module developed and used in this article. Based on the input value of Z_{min} of each battery cell, the ANN-based capacity estimator (Section II-A) outputs the estimated available capacity Q_{avail} to calculate or correct SOC value of each battery cell or battery module. The SOC value for each battery cell is calculated as given by the following equation:

$$\text{SOC} = \frac{Q_{\text{avail}} - \sum I_{\text{batt}} \Delta t}{Q_{\text{nominal}}} \tag{7}$$

where Q_{avail} is the estimated available capacity of the battery cell or battery module, I_{batt} is the current of the battery cell, and Δt is the time interval during which the battery cell current is equal to I_{batt}. Because of the ANN-based capacity estimation functionality, the relatively healthier battery cell has larger Q_{avail} than the Q_{avail} of the relatively unhealthy (or less healthy) battery cell. When the capacity estimation information/result is fed into the SOC balancing controller, it will create a difference among the values of SOC of battery cells to compensate the aging or health status differences of battery cells (refer to Fig. 6). As a result, the SOC value of a relatively less healthy battery will decrease. This makes the system draw less energy from the less healthy battery because of the mechanism of the designed SOC balancing controller, which is discussed next.

The reference value for the SOC balancing controller (Fig. 6), i.e., SOC_{ref}, is calculated as (8) shows

$$\text{SOC}_{\text{ref}} = \frac{(\text{SOC}_1 + \text{SOC}_2 + \cdots + \text{SOC}_i + \cdots + \text{SOC}_N)}{N} \tag{8}$$

where SOC_i is the SOC value of ith battery cell, and N is the number of batteries in the system. The output of SOC balancing controller is the voltage multiplier α_{vi} (I = 1,2,...,N) for each BPU. The value of α_{vi} is calculated based on the following equation:

$$\alpha_{vi} = 1 - (\text{SOC}_{\text{ref}} - \text{SOC}_i) \times G_{v\text{SOC}}(z) \tag{9}$$

where $G_{v\text{SOC}}(z)$ is the digital or discrete SOC balancing proportional-integral (PI) compensator/controller of the SOC control loop as given by the following equation:

$$G_{v\text{SOC}}(z) = K_{P-\text{SOC}} + \frac{K_{I-\text{SOC}} \times z}{z-1} \tag{10}$$

where $K_{P-\mathrm{SOC}}$ and $K_{I-\mathrm{SOC}}$ are the parameters of SOC balancing PI compensator. In the experimental work of this article, the used values for $K_{P-\mathrm{SOC}}$ and $K_{I-\mathrm{SOC}}$ are equal to 99.9 and 0.2, respectively, and the SOC value used by the SOC control loop is sampled at $f_{\mathrm{SOC}} = 1/T_{\mathrm{SOC}} = 1$ sample/second (i.e., $T_{\mathrm{SOC}} = 1$ s).

The voltage multiplier α_{vi} is used to decide the output voltage reference value of dc–dc converter connected with each battery cell, and the output voltage reference value $V_{i-\mathrm{ref}}$ (i = 1,2,...,N) is calculated as (11) shows

$$V_{i-\mathrm{ref}} = \frac{\alpha_{vi}}{M_v} \times V_{\mathrm{Bus-ref}} = \frac{\alpha_{vi}}{\alpha_{v1} + \alpha_{v2} + \ldots + \alpha_{vN}} \times V_{\mathrm{Bus-ref}} \quad (11)$$

where $V_{\mathrm{Bus-ref}}$ is the reference value of bus voltage, i.e., V_{Bus}, as shown in Fig. 1 and M_v is the sum of all the voltage multiplier values as given by the following equation:

$$M_v = \alpha_{v1} + \alpha_{v2} + \ldots + \alpha_{vN}. \quad (12)$$

Because the outputs of the dc–dc converters are connected in series in this article, the power drawn by load, i.e., P_{bus}, can be calculated as (13) shows

$$P_{\mathrm{bus}} = \sum_{i=1}^{N} p_i = \sum_{i=1}^{N} I_{\mathrm{bus}} V_i \quad (13)$$

where p_i is the output power of the ith BPU, I_{bus} is the bus current, and V_i is the output voltage of ith BPU or dc–dc converter. Then the power from the ith battery, i.e., $P_{\mathrm{batt}-i}$, can be calculated as (14) shows

$$P_{\mathrm{batt}-i} = \frac{P_i}{\eta_i} = \frac{I_{\mathrm{bus}} V_i}{\eta_i} = \frac{I_{\mathrm{bus}}}{\eta_i} \times V_{i-\mathrm{ref}} = k \times V_{i-\mathrm{ref}} \quad (14)$$

where η_i is the efficiency of the ith dc−dc power converter. The efficiency values of the dc−dc converters are assumed to be equal here for the purpose of theoretical analysis, i.e., every dc−dc converter is assumed to be identical, and the output voltage V_i is regulated to be equal to the reference value $V_{i-\mathrm{ref}}$ by the output voltage controller. Then based on (14), it can be noted that the higher the output voltage reference value is, i.e., $V_{i-\mathrm{ref}}$, the higher the power drawn from a battery cell, i.e., $P_{\mathrm{batt}-i}$, will be (the value of k here is a constant).

The duty cycle D_i of ith dc–dc converter is calculated as (15) shows

$$D_i = (V_{i-\mathrm{ref}} - V_i) \times G_{vB}(z) \quad (15)$$

where $G_{vB}(z)$ is the digital or discrete dc–dc converter output voltage PI compensator/controller as given by the following equation:

$$G_{vB}(z) = K_{P-vB} + \frac{K_{I-vB} \times z}{z - 1} \quad (16)$$

where K_{P-vB} and K_{I-vB} are the parameters of output voltage PI compensator. In the experimental work of this article, the used values for K_{P-vB} and K_{I-vB} are equal to 4.95 and 0.1, respectively, and the output voltage is sampled at $f_{vB} = 1/T_{vB} = 1$ Msample/second (i.e., $T_{vB} = 1$ μs).

Based on the above analysis, the SOC value of a relatively unhealthy or less healthy battery cell will decrease when the ANN-based capacity estimation is activated in the system. Therefore, the SOC balancing controller will output a smaller voltage multiplier for this corresponding less healthy battery cell. This causes the output voltage reference value for the dc−dc converter connected with this less healthy battery cell to decrease. Since all of the dc−dc converter outputs are connected in series and therefore carry the same output current, this results in less energy drawn from the less healthy battery cell, or more energy drawn from relatively healthier battery cell, in order for all of the battery cells to reach their end of discharge at the same time.

The SOC balancing controller sets the discharge rate for a given battery cell based on its relative health compared to the other battery cells (and not the absolute value of its health), which yields a more accurate health-aware SOC balancing performance.

III. Preliminary Experimental Evaluation Results

In order to test and evaluate the presented SOC balancing controller with the SOH awareness capability, a proof-of-concept (POC) experimental setup is developed in the laboratory. The Tenergy ICR 18650-2600 lithium-ion battery is used in this article, and its main specifications are: 4.2 V maximum voltage, 3.7 V nominal voltage, 2.6 Ah nominal capacity, and 65 mΩ initial internal impedance magnitude at 1 kHz [38]. TI microcontroller TMS320F28335 [39], [40] is used to calculate SOC values, implement the related SOC balancing control algorithm, and track the minimum complex impedance magnitude Z_{min} value of each battery cell. The ANN-based capacity estimation module is realized by python programming and carried out in the computer. The estimated capacity value, i.e., Q_{avail}, is sent from the ANN module to the TI microcontroller TMS320F28335 (using serial communication interface [41]). Each battery cell is connected at the input of the corresponding dc–dc boost converter [Fig. 4(a)]. The main parameters of interest of each dc−dc boost converter are: 4.7 μH inductor, 120 μF input and output capacitors, and 100 kHz switching frequency. The total bus voltage (Fig. 1) and bus current (i.e., load current) in this article as shown in Fig. 1 are set to 18 V and 1 A, respectively. One brand new battery (battery 1) and one aged battery (battery 2), i.e., which has a lower SOH, are selected for experiment in this article. These two batteries are charged fully (to 4.2 V each) before used for experiment in this article.

The layout design of the experimental prototype is made symmetric and uniform in order to minimize stray impedance values and make their effect uniform on the measurement of minimum impedance values across all battery cells.

Fig. 7 shows the battery impedance online measurement results (using the method described in Section II-B) which are then used for tracking the minimum impedance magnitude of battery 1 and battery 2 and used in the ANN estimation module (Section II-A). The impedance measurement is done at the beginning of discharging when each battery cell is almost at

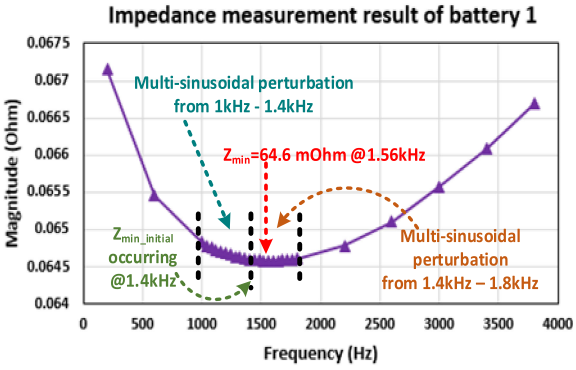

(a)

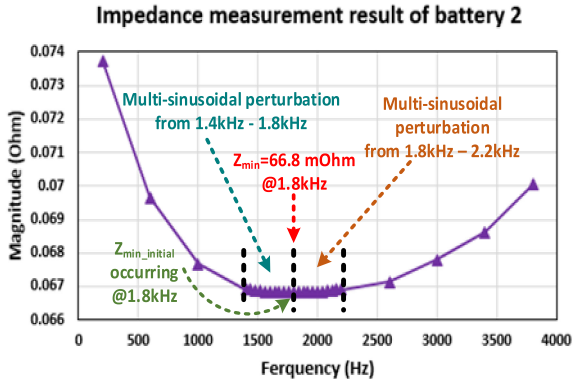

(b)

Fig. 7. Battery impedance measurement results for tracking the value of $Z_{\min}$. (a) Battery 1. (b) Battery 2.

its fully charged state (i.e., 100% SOC state). The frequency used for step-function perturbation is 200 Hz.

Based on the impedance measurements using the step-function perturbation, the initial minimum complex impedance magnitude values ($Z_{\text{min-initial}}$ as shown in Fig. 5) of battery 1 and battery 2 occur at 1.4 and 1.8 kHz, respectively. For battery 1, because the $Z_{\text{min-initial}}$ occurs at 1.4 kHz (i.e., $f_{\text{min-initial}}$ = 1.4 kHz), the value of k' is calculated to be 4 based on (4). The multisinusoidal perturbations are activated within two frequency ranges, i.e., 1−1.4 kHz and 1.4−1.8 kHz, and the multisinusoidal perturbation frequencies are calculated based on (5) and (6). By following the tracking algorithm presented in Section II-B, the tracked $Z_{\min}$ value of battery 1 is found to be equal to 64.6 mΩ at 1.56 kHz. For battery 2, because the $Z_{\text{min-initial}}$ occurs at 1.8 kHz (i.e., $f_{\text{min-initial}} = 1.8$ kHz), the value of k' is calculated to be 5 based on (4). The multisinusoidal perturbations are activated within two frequency ranges, i.e., 1.4−1.8 kHz and 1.8−2.2 kHz, and the multisinusoidal perturbation frequencies are determined based on (5) and (6). By following the tracking algorithm presented in Section II-B, the tracked $Z_{\min}$ value of battery 2 is found to be equal to 66.8 mΩ at 1.8 kHz. It can be observed that the value of $Z_{\min}$ for battery 2 is larger than the value of $Z_{\min}$ for battery 1, which is expected because battery 2 is older/aged and has a lower SOH.

A total of 990 data samples are used for initial training of the ANN-based capacity estimator. The 990 data points are collected using the battery aging experiment conducted on the aging platform presented in [5]. The complete dataset of samples can be treated as a two-dimensional array of data structure (X, Y) = ($Z_{\min}$, Q_{avail}).

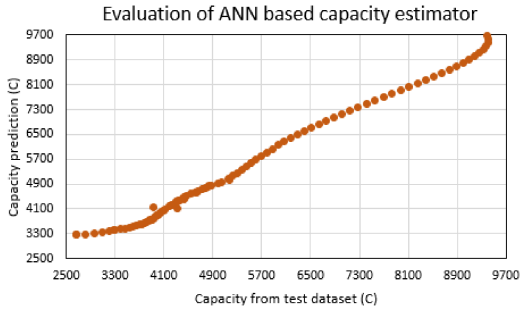

Fig. 8. Evaluation results of ANN-based capacity estimator on the test dataset.

Eight hundred and eighty data points of the 990 data points are used for k-fold cross-validation dataset, and the remainder 110 data points are used for test dataset. The k value is chosen to be 10 for the k-fold cross-validation and the threshold value for the average validation error is set to be 300 Coulombs (C). The trained ANN-based capacity estimator is evaluated by the test dataset, and the evaluation result is shown in Fig. 8. The average absolute magnitude error on the test dataset is 110.8 C, which is about 2.61%. The estimation relative error is calculated as follows:

$$\text{relative error} = \frac{|Q_{\text{pred}} - Q_{\text{test}}|}{Q_{\text{test}}} \times 100\% \qquad (17)$$

where Q_{pred} is the predicted available capacity given by the ANN-based capacity estimator and Q_{test} is the capacity value from the test dataset. Based on these results, the evaluation score on the test dataset is fairly good. This means the developed or trained ANN-based capacity estimator can predict battery available capacity fairly well. Based on the tracked $Z_{\min}$ values of battery 1 and battery 2, the predicted available capacity values by the ANN-based available capacity estimator for battery 1 and battery 2 are 9360 and 8017 C, respectively, where 9360 C corresponds to $Z_{\min}$ = 64.6 mΩ and 8017 C corresponds to $Z_{\min}$ = 66.8 mΩ. This indicates that the available capacity of battery 2 is ∼14.35% lower than the available capacity of battery 1.

Fig. 9 shows the values of SOC, α_v, and $V_{i\text{-ref}}$ (in Fig. 6) for each of the two batteries during discharging, when the SOH effect is accounted for by the controller [Fig. 9(a), (b), and (c), respectively] and when the SOH effect is not accounted for by the controller [Fig. 9(d), (e), and (f), respectively]. In Fig. 9(a), from t = 0 to t = 6 min, the SOH effect of battery cells is initially not accounted for and the capacity capabilities of both battery cells are assumed to be the same (SOH difference between the two batteries is not accounted for yet). However, at t = 6 min, the capacity capabilities of battery 1 and battery 2 are corrected based on the estimation results from the ANN-based capacity estimator (i.e., the system becomes aware of the actual available capacity capability based on the SOH information), and the corrected available capacity values are fed to the SOC balancing

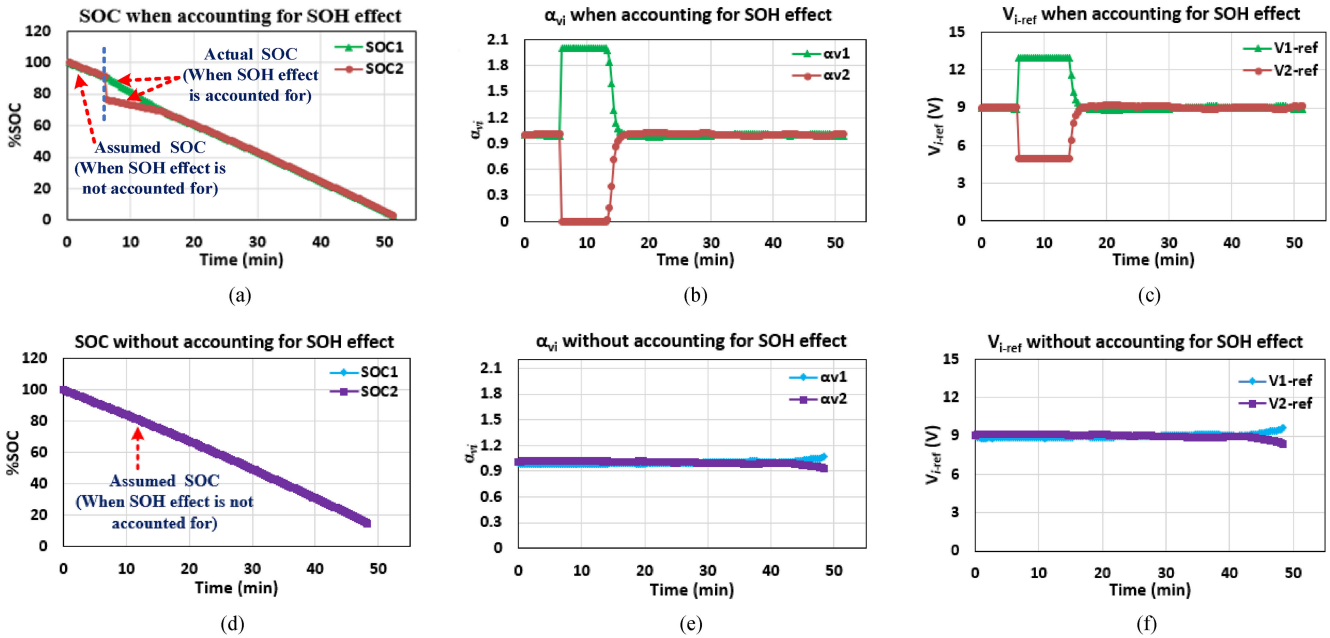

Fig. 9. Experimentally measured values of SOC, α_v and $V_{i\text{-ref}}$ for each of the two batteries during discharging. (a) SOC values when SOH effect is accounted for by the controller. (b) α_v values when SOH effect is accounted for by the controller. (c) $V_{i\text{-ref}}$ values when SOH effect is accounted for by the controller. (d) SOC values when SOH effect is not accounted for by the controller. (e) α_v values when SOH effect is not accounted for by the controller. (f) $V_{i\text{-ref}}$ values when SOH effect is not accounted for by the controller.

controller. Because of this capacity capability correction or adjustment, the SOC value [Fig. 9(a)] of battery 2 is corrected from 90.9% to 76.2%, and the SOC value of battery 1 is almost not changed (from 90.9% to 90.3%). This adjustment yields ∼14.1% SOC value difference between battery 1 and battery 2. As a result and based on (9) and Fig. 6, the SOC balancing controller outputs larger voltage multiplier α_{v1} for battery 1 and smaller voltage multiplier α_{v2} for battery 2 as shown in the results in Fig. 9(b) until the SOC is balanced at $t = 15$ min (9 min after $t = 6$ min). After this time, the multiplier values might maintain slight mismatch in order to keep balanced SOC values.

Based on the α_{v1} and α_{v2} values, the output voltage reference values $V_{1\text{-}ref}$ and $V_{2\text{-}ref}$ for each dc–dc converter connected with each battery are calculated according to (11). The limits set in microcontroller for the values of α_v and $V_{i\text{-ref}}$ for this design are given by (18) and (19), respectively. From $t = 6$ min to $t = \sim$14 min, α_{v1} and α_{v2} values reach their limits of 2 and 0, respectively, and the corresponding $V_{1\text{-ref}}$ and $V_{2\text{-ref}}$ values reach their limit of 13 and 5 V, respectively. This allows the system to draw higher power from battery 1 and lower power from battery 2. The SOC values of the two batteries are balanced around $t = 15$ min, and the balance is maintained until the end of discharging operation. The system stops discharging operation when one of the following conditions occurs: 1) the SOC value of one of the battery cells reaches zero or 2) when the voltage of one of battery cells reaches the discharge end voltage of 2.7 V [38] in order to prevent over-discharging of any of the battery cells. Under this case experiment, the system stopped discharging operation at $t = 51.3$ min when the voltage of battery 1 reaches the discharge end voltage. This occurred when the SOC values of battery 1 and battery 2 were equal to 0.89% and 1.19%, respectively

$$\alpha_{vi} = \begin{cases} 0, & \text{if } \alpha_{vi} \le 0 \\ \alpha_{vi}, & \text{if } 0 < \alpha_{vi} < 2 \\ 2, & \text{if } \alpha_{vi} \ge 2 \end{cases} \tag{18}$$

$$V_{i-\text{ref}} = \begin{cases} 5V, & \text{if } V_{i-\text{ref}} \le 5V \\ V_{i-\text{ref}}, & \text{if } 5\text{V} < V_{i-\text{ref}} < 13V. \\ 13V, & \text{if } V_{i-\text{ref}} \ge 13V \end{cases} \tag{19}$$

The results plotted in Fig. 9(d), (e), and (f) are for the case when the SOH effected is not accounted for, i.e., the SOH estimation result is not fed to the SOC balancing controller (in this case, in Fig. 6, $Q_{\text{avail}-1} = Q_{\text{avail}-2}$ for battery 1 and battery 2, which is, in fact, not the case because the SOH for battery 2 is lower than the SOH for battery 1). In this case, battery 2, which is the battery with lower SOH, reached the discharge end voltage or end of discharging earlier than battery 1 and therefore the controller terminated the operation earlier at $t = 48.3$ min. At the end of operation in this case, 13.6% of battery 1 SOC value has not been used due to early termination to protect battery 2 from over-discharging. The difference between the values of α_{v1} and α_{v2} and the difference between the values of $V_{1\text{-}ref}$ and $V_{2\text{-}ref}$ at the end of operation are because the voltage of battery 2 drops very quickly at the end and is much smaller than that of battery 1 and the controller is attempting to correct the voltage references to maintain SOC balance under different battery voltages.

Fig. 10 shows the experimental measured voltages, currents, and used/discharged coulombs for each of the two battery cells when the SOH effect is accounted for by the controller and when the SOH effect is not accounted for by the controller. For the

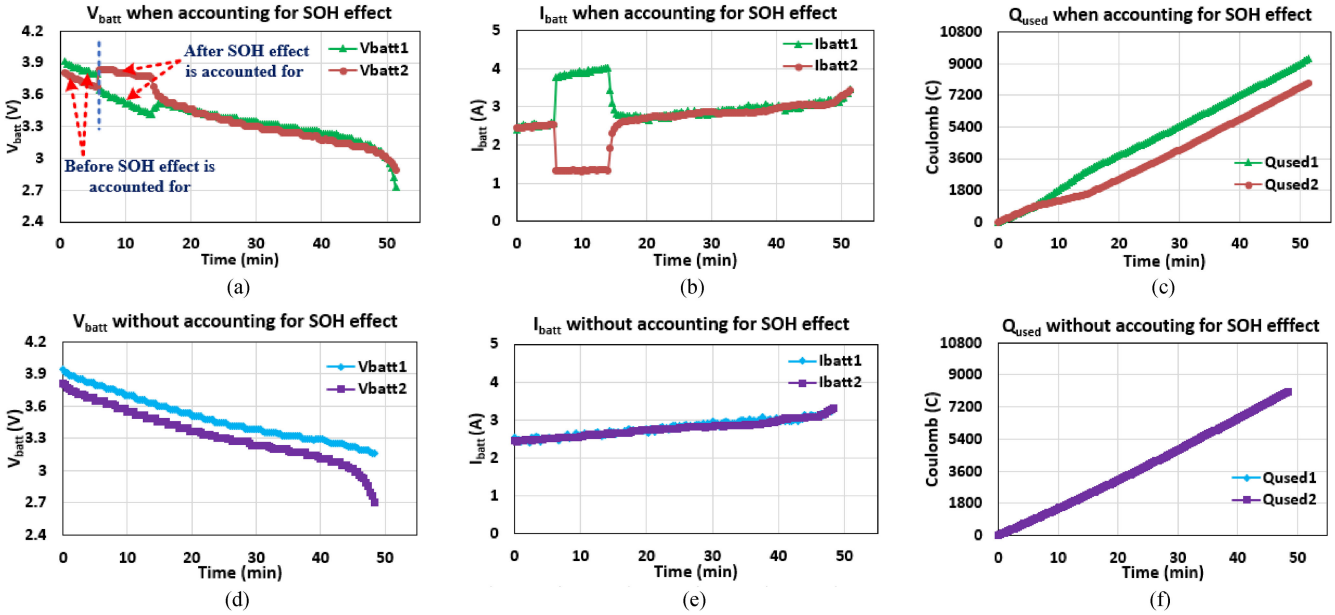

Fig. 10. Experimentally measured voltages, currents, and used/discharged coulombs during the discharging operation for the two battery cells. (a) Battery cell voltages when SOH effect is accounted for by the controller. (b) Battery cell currents when SOH effect is accounted for by the controller. (c) Used/discharged coulombs when SOH effect is accounted for by the controller. (d) Battery cell voltages when SOH effect is not accounted for by the controller. (e) Battery cell currents when SOH effect is not accounted for by the controller. (f) Used/discharged coulombs when SOH effect is not accounted for by the controller.

TABLE II
PERFORMANCE COMPARISON BETWEEN THE CASE WHEN SOH EFFECT IS ACCOUNTED FOR AND THE CASE WHEN SOH EFFECT IS NOT ACCOUNTED FOR BY THE CONTROLLER

Case	System operation time (min)	Coulomb utilization (C)	Battery 1			Battery 2		
			Voltage at the end (V)	Coulombs discharged (C)	Estimated capacity (C)	Voltage at the end (V)	Coulombs discharged (C)	Estimated capacity (C)
When accounting for SOH effect	51.3	17181	2.724	9276	9360	2.892	7905	8017
Without accounting for SOH effect	48.3	16171	3.164	8084	9360	2.703	8087	8017

case when SOH effect is accounted for by the controller, the value of V_{batt1} becomes almost equal to the value of V_{batt2} after the capacity capabilities of batteries are corrected/adjusted by the ANN capacity/SOH estimator using EIS data and the SOC values are rebalanced. By the end of discharge operation, the used coulombs/capacities from battery 1 and battery 2 are 9276 and 7905 C, respectively, in this case, which are very close to the estimated capacity value of battery 1 and battery 2, i.e., 9360 and 8017 C, respectively.

For the case when SOH effect is not accounted for by the controller, the value of V_{batt1} is larger than the value of V_{batt2} during the entire operation. This can partially be explained by the following equation:

$$V_{\text{terminal}} = V_{\text{ocv}} - I_{\text{batt}} \times Z \tag{20}$$

where V_{terminal} is the terminal voltage of the battery which is represented by the voltages (V_{batt1} and V_{batt2}) shown in Fig. 10(a) and (d), V_{ocv} is the open circuit voltage of the battery, and Z is the magnitude of battery impedance. As discussed and shown earlier in this article, battery 2 is moderately aged battery, and its impedance magnitude is larger than that of battery 1 (new battery). This explains why V_{batt2} is smaller than V_{batt1} in Fig. 10(d) even though both batteries are charged fully to 4.2 V before discharging experiment and I_{batt1} is equal to I_{batt2} during the discharging (when SOH is not accounted for by the controller). Under this case when SOH effect is not accounted for by the controller, the used/discharged coulombs/capacities from battery 1 and battery 2 are 8084 and 8087 C, respectively.

Table II summarizes some of the results and shows a comparison between the case when the SOH effect is accounted for in the SOC balancing controller and the case when the SOH effect is not accounted for in the SOC balancing controller. The presented SOC balancing method with SOH awareness using impedance information has the following advantages.

1) It extends the system operation time. In the experimental example of this article, the operation is extended from 48.3 to 51.3 min, which is a 6.21% improvement.
2) It improves the energy/coulomb utilization efficiency. In the example system of this article, when the controller accounts for the SOH effect, the system can draw a total of ∼17 181 C from the two batteries (9276 C from battery 1 and 7905 C from battery 2) compared to ∼16 171 C when

SOH is not accounted for. This yields 6.25% (1010 C) improvement.

3) Instead of assuming that each battery cell or module has the same capacity capability, the ANN capacity/SOH estimator using the impedance information results in a more accurate capacity estimation and therefore SOC estimation.
4) It reduces the possibility of over-discharging issue in the battery system.

IV. Conclusion

The presented SOC balancing controller has an SOH awareness and it takes the SOH status for each lithium-ion battery cell or module into consideration in its operation, which yields several advantages such as increased operation time, energy utilization efficiency, and avoidance of over-discharging. The avoidance of over-discharging can maintain batteries healthier for longer time and reduces the possibility of catastrophic failures.

The presented ANN-based capacity/SOH estimator which utilizes the relationship between the minimum complex impedance magnitude value of the battery and capacity fading yields fairly good SOH estimation results in order to have accurate SOC estimation or calculation. The presented hybrid online battery impedance measurement method with higher speed and higher measurement resolution allows the ANN-based capacity/SOH estimator to quickly and accurately obtain the minimum complex impedance magnitude value of the battery in order to quickly estimate SOH. This provides the ANN-based SOH estimator to quickly see any change in SOH values during operation without needing to wait for one or several operation cycles to see such change.

The operation of the presented SOC balancing controller with SOH awareness is evaluated using a POC experimental setup. The results demonstrated the operation of the system and its potential.

The advances in the technology of high-speed digital circuits and microcontrollers have made the implementation of complex calculations and functions easier, faster, and with a cost that continues to decrease. For example, using the relatively low-cost microcontroller TI TMS320F28335 [39], [40] in this article, which has a clock speed of 150 MHz and 16 ADC channels, the process for finding the minimum impedance value and available capacity does not take more than a few seconds (note that SOC and SOH are slowly varying parameters that are updated at low speed). The added cost as a result of adding the presented controller to a battery system is expected to be relatively low compared to the overall cost of the battery system and the resulted performance advantages such as increased reliability, safety, and operation lifetime. It should be noted that the presented controller does not need to be realized at the cell level and can be realized at the battery module level in order to reduce the added cost (i.e., a battery module can, for example, include 10 battery cells connected in series and one minimum impedance value is found for the module as if they were one larger battery cell). In this case, the health-aware SOC balancing control can be achieved between several battery modules.

Future work includes, but is not limited to, studying other SOH indicators for SOH estimation and developing ANN-based SOH or capacity estimators with multi-SOH indicators as its inputs to utilize the advantages of each SOH indicator and then to achieve better battery SOH/capacity capability estimation performance.

References

[1] Z. Xia and J. A. Abu Qahouq, "Adaptive and fast state of health estimation method for lithium-ion batteries using online complex impedance and artificial neural network," in *Proc. IEEE Appl. Power Electron. Conf. Expo.*, Anaheim, CA, USA, Mar. 2019, pp. 3361–3365.

[2] P. J. Chauhan, B. D. Reddy, S. Bhandari, and S. K. Panda, "Battery energy storage for seamless transitions of wind generator in standalone microgrid," *IEEE Trans. Ind. Appl.*, vol. 55, no. 1, pp. 69–77, Jan./Feb. 2019.

[3] V. Rallabandi, O. M. Akeyo, N. Jewell, and D. M. Ionel, "Incorporating battery energy storage systems into multi-MW grid connected PV systems," *IEEE Trans. Ind. Appl.*, vol. 55, no. 1, pp. 638–647, Jan./Feb. 2019.

[4] Z. N. Bako, M. A. Tankari, G. Lefebvre, and A. S. Maiga, "Experiment-based methodology of kinetic battery modeling for energy storage," *IEEE Trans. Ind. Appl.*, vol. 55, no. 1, pp. 593–599, Jan./Feb. 2019.

[5] Z. Xia, J. A. Abu Qahouq, E. Phillips, and R. Gentry, "A simple and upgradable autonomous battery aging evaluation and test system with capacity fading and AC impedance spectroscopy measurement," in *Proc. IEEE Appl. Power Electron. Conf. Expo.*, Tampa, FL, USA, Mar. 2017, pp. 951–958.

[6] D. Bazargan, S. Filizadeh, and A. M. Gole, "Stability analysis of converter-connected battery energy storage systems in the grid," *IEEE Trans. Sustain. Energy*, vol. 5, no. 4, pp. 1204–1212, Oct. 2014.

[7] M. S. H. Lipu, M. A. Hannan, A. Hussain, M. H. Saad, A. Ayob, and M. N. Uddin, "Extreme learning machine model for state-of-charge estimation of lithium-ion battery using gravitational search algorithm," *IEEE Trans. Ind. Appl.*, vol. 55, no. 4, pp. 4225–4234, Jul./Aug. 2019.

[8] S. M. Chowdhury, M. O. Badawy, Y. Sozer, and J. A. D. A. Garcia, "A novel battery management system using the duality of the adaptive droop control theory," *IEEE Trans. Ind. Appl.*, vol. 55, no. 5, pp. 5078–5088, Sep./Oct. 2019.

[9] S. Yarlagadda, T. Hartley, and I. Husain, "A battery management system using an active charge equalization technique based on a DC/DC converter topology," *IEEE Trans. Ind. Appl.*, vol. 49, no. 6, pp. 2720–2729, Nov./Dec. 2013.

[10] J. Qi and D. D. Lu, "Review of battery cell balancing techniques," in *Proc. Australas. Universities Power Eng. Conf.*, Sep. 2014, pp. 1–6.

[11] Y. Shang, C. Zhu, Y. Fu, and C. Mi, "An integrated heater equalizer for lithium-ion batteries of electric vehicles," *IEEE Trans. Ind. Appl.*, vol. 66, no. 6, pp. 4398–4405, Jun. 2019.

[12] W. Huang and J. A. Abu Qahouq, "Energy sharing control scheme for state-of-charge balancing of distributed battery energy storage system," *IEEE Trans. Ind. Electron.*, vol. 62, no. 5, pp. 2764–2776, May 2015.

[13] Y. Yuanmao, K. W. E. Chen, and Y. P. B. Yeung, "Zero-current switching switched-capacitor zero-voltage-gap automatic equalization system for series battery string," *IEEE Trans. Power Electron.*, vol. 27, no. 7, pp. 3234–3242, Dec. 2011.

[14] S. Li, C. C. Mi, and M. Zhang, "A high-efficiency active battery-balancing circuit using multiwinding transformer," *IEEE Trans. Ind. Appl.*, vol. 49, no. 1, pp. 198–207, Jan./Feb. 2013.

[15] C. Young, N. Chu, L. Chen, Y. Hsiao, and C. Li, "A single-phase multilevel inverter with battery balancing," *IEEE Trans. Ind. Electron.*, vol. 60, vv no. 5, pp. 1972–1978, May 2013.

[16] B. Ge, Y. Liu, H. Abu-Rub, and F. Z. Peng, "State-of-charge balancing control for a battery-energy-stored quasi-z-source cascaded-multilevel-inverter-based photovoltaic power system," *IEEE Trans. Ind. Electron.*, vol. 65, no. 3, pp. 2268–2279, Mar. 2018.
[17] C. Pinto, J. V. Barreras, E. Schaltz, and R. E. Araujo, "Evaluation of advanced control for li-ion battery balancing systems using convex optimization," *IEEE Trans. Sustain. Energy*, vol. 7, no. 4, pp. 1703–1717, Oct. 2016.
[18] K. M. Lee, Y. C. Chung, C. H. Sung, and B. Kang, "Active cell balancing of Li-ion batteries using LC series resonant circuit," *IEEE Trans. Ind. Electron.*, vol. 62, no. 9, pp. 5491–5501, Sep. 2015.
[19] X. Cao, Q. Zhong, Y. Qiao, and Z. Deng, "Multilayer modular balancing strategy for individual cells in a battery pack," *IEEE Trans. Energy Convers.*, vol. 33, no. 2, pp. 1703–1717, Jun. 2018.
[20] H. Zhang, Y. Wang, and J. Zhang, "Active battery equalization method based on redundant battery for electric vehicles," *IEEE Trans. Veh. Technol.*, vol. 68, no. 8, pp. 7531–7543, Aug. 2019.
[21] L. Maharjan, S. Inoue, H. Akagi, and J. Asakura, "State-of-charge (SOC)-balancing control of a battery energy storage system based on a cascade PWM converter," *IEEE Trans. Power Electron.*, vol. 24, no. 6, pp. 1628–1636, Jun. 2009.
[22] C. Weng, J. Sun, and H. Peng, "Model parametrization and adaptation based on the invariance of support vectors with applications to battery state-of-health monitoring," *IEEE Trans. Veh. Technol.*, vol. 64, no. 9, pp. 3908–3917, Sep. 2015.
[23] T. Kim *et al.*, "An on-board model-based condition monitoring for lithium-ion batteries," *IEEE Trans. Ind. Appl.*, vol. 55, no. 2, pp. 1835–1843, Mar./Apr. 2019.
[24] H. Yuan and L. Dung, "Offline state-of-health estimation for high-power lithium-ion batteries using three-point impedance extraction method," *IEEE Trans. Veh. Technol.*, vol. 66, no. 3, pp. 2019–2032, Mar. 2017.
[25] A. Guha and A. Patra, "State of health estimation of lithium-ion batteries using capacity fade and internal resistance growth models," *IEEE Trans. Transp. Electrific.*, vol. 4, no. 1, pp. 135–146, Nov. 2017.
[26] N. Li, F. Gao, T. Hao, Z. Ma, and C. Zhang, "SOH balancing control method for MMC battery energy storage system," *IEEE Trans. Ind. Electron.*, vol. 99, no. 99, pp. 1–1, Aug. 2017.
[27] J. Kim, H. Chun, M. Kim, J. Yu, T. Kim, and S. Han, "Data-driven state of health estimation of Li-ion batteries with RPT-reduced experimental data," *IEEE Access*, vol. 7, pp. 106987–106997, Aug. 2019.
[28] J. A. Abu Qahouq and Z. Xia, "Single-perturbation-cycle online battery impedance spectrum measurement method with closed-loop control of power converter," *IEEE Trans. Ind. Electron.*, vol. 64, no. 9, pp. 7019–7029, Sep. 2017.
[29] W. Huang and J. A. Abu Qahouq, "An online battery impedance measurement method using DC-DC power converter control," *IEEE Trans. Ind. Electron.*, vol. 61, no. 11, pp. 5987–5995, Nov. 2014.
[30] W. Waag, S. Käbitz, and D. Sauer, "Experimental investigation of the lithium-ion battery impedance characteristic at various conditions and aging states and its influence on the application," *Appl. Energy*, vol. 102, pp. 885–897, Feb. 2013.
[31] M. Mese and P. Vaidyanathan, "Look-up table (LUT) method for inverse half toning," *IEEE Trans. Image Process.*, vol. 10, no. 10, pp. 1566–1578, Oct. 2001.
[32] M. Abdulkarim, A. Shafie, W. Ahmad, and R. Razali, "Performance comparison between MLP neural network and exponential curve fitting on airwaves data," in *Proc. Adv. Comput. Sci. Appl.*, Heidelberg, Berlin, Germany, 2014, pp. 1079–1087.
[33] H. Anysz, A. Zbiciak, and N. Ibadov, "The influence of input data standardization method on prediction accuracy of artificial neural networks," *Proc. Eng.*, vol. 153, pp. 66–70, Aug. 2016.
[34] J. Lei, "Cross-validation with confidence," *J. Amer. Stat. Assoc.*, vol. 00, no. 0, pp. 1–20, Oct. 2019.
[35] V. Nair and G. E. Hinton, "Rectified linear units improve restricted Boltzmann machines," in *Proc. Int. Conf. Mach. Learn.*, Haifa, Israel, Jun. 2010, pp. 807–814.
[36] N. Shobha and T. Asha, "Mean squared error applied in back propagation for nonlinear rainfall prediction," *Compusoft*, vol. 8, no. 9, pp. 3431–3439, Sep. 2019.
[37] M. C. Mukkamala and M. Hein, "Variants of RMSProp and Adagrad with logarithmic regret bounds," in *Proc. Int. Conf. Mach. Learn.*, Sydney, NSW, Australia, Aug. 2017, pp. 2545–2553.
[38] Tenergy Corp., *Cylindric Lithium-Ion Cell 30005-0*, Datasheet of Tenergy. Accessed: Jul. 18, 2020. [Online]. Available: https://www.shorepowerinc.com/media/wysiwyg/files/Tenergy-30005-0-datasheet.pdf
[39] Texas Instruments Inc., *Datasheet of TMS320F28335 Microcontroller*. Accessed: Dec. 24, 2019. [Online]. Available: https://www.ti.com/product/TMS320F28335
[40] Texas Instruments Inc., *TMS320F28335 Ordering & Quality*. Accessed: Jul. 18, 2020. [Online]. Available: https://www.ti.com/product/TMS320F28335#order-quality
[41] Texas Instruments Inc., *Datasheet of TMS320x2833x, 2823x Serial Communications Interface (SCI)*. Accessed: Dec. 24, 2019. [Online]. Available: http://www.ti.com/lit/ug/sprufz5a/sprufz5a.pdf